J Electroceram (2007) 18:57–65
DOI 10.1007/s10832-007-9008-7

Synthesis and characterization of nanocrystalline Barium Strontium Titanate powder via sol-gel processing

Vikas Somani · Samar Jyoti Kalita

Received: 16 May 2005 / Accepted: 23 May 2006 / Published online: 15 February 2007
© Springer Science + Business Media, LLC 2007

Abstract Barium Strontium Titanate (BST) solid solution is a strong candidate material for application in tunable ferroelectric devices. In this research, we have synthesized and characterized nanocrystalline BST ($Ba_{0.7}Sr_{0.3}TiO_3$) powder with average particle-diameter of 15 nm through a simple sol-gel process, using barium acetate, strontium acetate and titanium isopropoxide as the precursors. In this process, stoichiometric proportions of barium acetate and strontium acetate were dissolved in acetic acid followed by refluxing, and addition of titanium (IV) isopropoxide to form BST gel. The gel was analyzed using Differential Scanning Calorimetry (DSC) and Thermal Gravimetric Analysis (TGA). The as-formed gel was dried at 200 °C and then calcined in the temperature range of 400 to 800 °C for crystallization. Phase evolution during calcination was studied using X-ray diffraction (XRD) technique. Particle size, morphology and the lattice fringes of the calcined powder were characterized by high-resolution transmission electron microscopy (HR-TEM). To study the effects of sintering on BST nanopowder, green ceramic specimens were prepared by uniaxial compaction and then sintered at 950–1,100 °C under atmospheric conditions. Sintered specimens were analyzed for phase composition, grain size and geometric bulk density.

Keywords Barium Strontium Titanate · Nanopowder-synthesis · Nano-electroceramics · Sintering · Sol-gel

V. Somani · S. J. Kalita (✉)
Department of Mechanical, Materials and Aerospace Engineering,
University of Central Florida,
Orlando, FL 32816-2450, USA
e-mail: samar@mail.ucf.edu

1 Introduction

A number of titanate-based ferroelectric materials have been investigated in the past for tunable device applications. These ferroelectrics are used as phase shifters, resonators, filters and capacitors in communication systems [1, 2]. The solid solution of Barium Strontium Titanate (BST) has emerged as a strong candidate material for such applications. $Ba_xSr_{1-x}TiO_3$ is a continuous solid solution between $BaTiO_3$ and $SrTiO_3$ over its entire composition range [3]. Dielectric permittivity of BST is dependent on composition and tem>perature and, can be tuned on application of a DC electric field [4]. BST exhibits a maximum dielectric permittivity in the temperature range 0–390 K [5] and possesses attractive properties required for tunable applications [6].

The dielectric constant and intrinsic losses of ferroelectric materials depend on their process of synthesis, microstructure and, dopants used [7, 8]. Various processes like sputtering, laser ablation, chemical vapor deposition (CVD), solid-state processing and sol-gel have been used to synthesize BST powder and its thin films for ferroelectric applications. However, there is still a need to evolve better process and technology to synthesize reliable tunable material, with reduced dielectric constant and material loss tangent; while possessing higher tunability so as to get optimum K factor (tunability/loss tangent). Some of these existing challenges and needs might find solution in the arena of nano-technology and nano-materials, which exhibit some of the extraordinary properties due to their unusual chemical and/or synergistic properties. In order to make ferroelectric materials compatible to semiconductor processing techniques nano range thin films is a necessity. High frequency thin film BST device design is generally based on two approaches. The first uses thin films of thickness

<50 nm and the second approach uses thicker films generally >300 nm [9]. Thin films of BST doped with magnesium have been synthesized with an average grain size of 25 nm, low dielectric loss of 0.007 and dielectric constant of 386 [10].

Sol-gel synthesis of tunable, non-linear dielectric materials offer advantages like low temperature synthesis, ease in controlling the composition variations, low cost and potential use in film processing. It is believed that nano-sized materials can offer modified electron sensitive properties [11] and better sinterability [12]. Earlier studies on synthesis of crystalline BST powder resulted in powder of 0.8–2.7 μm [13] using a solid-state reaction route. Selvam and Kumar [14] reported the synthesis of 50 nm BST powder by direct precipitation method. Shen et al. [15] successfully synthesized 100 nm BST powder using nitrate based precursor solutions. Addition of ethyl alcohol during the process further reduced the powder grain size.

Widespread application of BST for use as parallel plate capacitor in tunable microwave devices demand good sintering characteristic at low temperatures of around 900 °C. This would also enable the use of BST in low temperature co-fired ceramic (LTCC) structures [16]. Nanocrystalline powder, because of their high diffusivity, can be sintered at lower temperatures compared to their polycrystalline coarse grain counterparts [17]. Consequently, in order to meet the two requirements of thin film applicability and low sintering temperatures, there is a need for nanocrystalline BST powder with improved properties. Nanoscale BST powder can also be used to fabricate ferroelectric particle dispersed nanocomposites exhibiting intelligent functions like predicting and controlling of crack initiation and growth [18].

The objective of this research was to synthesize nanocrystalline BST powder below 20 nm via a simple sol-gel process, which could be easily reproduced and, to study its sintering behavior. Synthesis of highly crystalline BST nanopowder with an average particle size of 15 nm, after calcination at 700 °C, was successfully accomplished. DSC and TGA were performed on the as-prepared thick gel. XRD and HR-TEM techniques were used to characterize the nanopowder. The phase evolution during crystallization was studied. Sintering studies were conducted to analyze the effect of elevated temperature on phase composition/transformation and densification. This paper presents a detailed description of our synthesis process and characterization activities.

2 Experimental procedure

2.1 Powder synthesis

$Ba_{0.7}Sr_{0.3}TiO_3$ nanopowder was synthesized using barium acetate (reagent grade, Acros Organics, NJ, USA), strontium acetate (reagent grade, Alfa Aesar, MA, USA) and titanium (IV) isopropoxide (purity 98 +%, Acros Organics, NJ, USA) as precursors for barium, strontium and titanium, respectively. Acetic acid (5% v/v Fisher scientific, USA) was used as solvent and 2-methoxy ethanol (99 +%, Acros Organics, New Jersey, USA) was used to stabilize Titanium (IV) isopropoxide. Stoichiometric proportions of barium acetate (0.08 mol) and strontium acetate (0.034 mol) powder were dissolved in 10 and 5 ml of acetic acid, respectively, by continuous magnetic stirring at 300 rpm for 15 min. The two solutions were then mixed and refluxed at 125 °C for 2 h. 2-Methoxy ethanol (2–4 ml) was added in Titanium (IV) isopropoxide (0.11 mol) to form a separate solution at room temperature. The Ba–Sr solution was added to the as-prepared Ti solution, in drops, with the help of a burette. pH of the solution was maintained in the range of 3.5–5 by adding buffering agents. Refluxing resulted in the formation of a thick white colored gel. De-ionized water was added to it and the solution was stirred magnetically for 30 min. This solution was then filtered and heated to 200 °C for 2 h, resulting in the formation of amorphous $Ba_{0.7}Sr_{0.3}TiO_3$ powder. The amorphous powder was then calcined at 400, 600 and 700 °C, separately, in a muffle furnace in atmospheric conditions, for crystallization. Figure 1 presents a schematic of the process showing synthesis of nanocrystalline BST powder.

2.2 Characterization of BST nanopowder

The as-formed BST gel was characterized using DSC and TGA to study its thermal properties. For this, 89 mg of as-

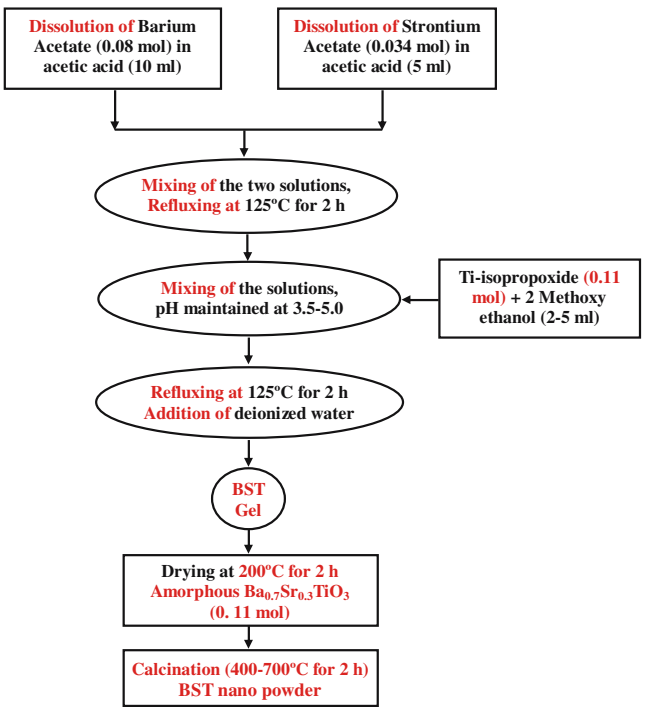

Fig. 1 Schematic detailing synthesis of nanocrystalline BST powder

processed gel sample was placed in the specimen holder of a GSC/TGA analyzer (Model SDT Q600 from TA Instruments, Inc.) and heated from ambient temperature to 1,100 °C. SDT Q600 provides reliable and accurate simultaneous measurement of heat flow and weight change from ambient temperature to 1,500 °C. Argon was used for purging at 10 ml/min. A heating rate of 6 °C/min was used.

BST powders calcined at different temperatures were characterized using XRD and HR-TEM techniques. Powder agglomerates heat-treated at 600 and 700 °C, were ground in a mortar and pestle to obtain fine powder. Phase analysis of the powder was conducted with the help of a Rigaku diffractometer (Model D/MAX-B, Rigaku Co., Tokyo, Japan) using Ni filtered CuKα radiation (λ=0.1542 nm) at 40 kV and 40 mA settings. The XRD patterns were recorded in the 2θ range of 20–40 degrees. The diffraction data were analyzed by Rietveld refinement techniques using General Structure Analysis System (GSAS) software [19]. GSAS is a set of programs for the processing and analysis of both single crystal and powder diffraction data obtained with X-rays or neutrons.

Based on XRD analysis, the powder calcined at 700 °C for 2 h was examined for its powder morphology, grain size and the lattice fringes using a HR-TEM (Model Tecnai—Philips F30, FEI Co., Hillsboro, OR). The calcined powder was ground into a fine powder and then dispersed in water by constant stirring for 15 min. A formvar-carbon coated copper grid was dipped into the solution and instantly withdrawn. This grid was used for HR-TEM analysis.

2.3 Powder consolidation and sintering

BST nanopowder calcined at 700 °C was uniaxially compacted in a cylindrical steel mold having 10 mm internal diameter, using a hydraulic single-action press from Carvar Inc. Green consolidated pellets, with average dimensions of 10 mm in diameter and 2.5 mm in thickness, were sintered in a high temperature programmable muffle furnace in ambient atmosphere at different temperatures (950, 1,000, 1,050, 1,100 °C) for 2 h. A heat treatment cycle was developed to allow better densification and avoid cracking. Pellets were initially heated to 400 °C at a heating rate of 5 °C/min and homogenized at this temperature for an hour. In the second step, temperature was increased to the desired final temperature at a slower heating rate of 2 °C/min. Soaking time to allow densification at the final temperature was 2 h. Pellets were cooled to room temperature at 8 °C/min. Three nano-BST specimens were heat-treated at each sintering temperature and the values reported are average of the three samples. Geometric bulk density (ρ_g) of each pellet was evaluated from the measurements of the mass of specimen and its volume (determined by dimensional measurements).

As-sintered BST structures at different sintering temperatures were ground into fine powder using a mortar and pestle for phase analysis. Phase analysis of the powder was conducted using Ni filtered CuKα radiation (λ=0.1542 nm) at 40 kV and 40 mA settings in a Rigaku diffractometer. The XRD patterns were recorded in the 2θ range of 20–36 degrees. The effect of elevated temperature on phase composition/transformation was studied using the XRD patterns recorded for BST sintered at 950, 1,000, 1,050 and 1,100 °C, for 2 h.

3 Results and discussion

3.1 Phase analysis of BST nano-powder

Figure 2 shows the XRD patterns of the powder calcined in air at 600 and 700 °C for 2 h, separately. It is observed that peaks obtained at 600°C are not sharp indicating that particles are not fully crystallized. Thermal heat treatment with appropriate time and temperature can cause the amorphous phase to crystallize because the amorphous phase is thermodynamically metastable state. This is what we observed, when the calcination temperature was raised from 600 to 700 °C. As seen in Fig. 2, the peaks observed for powder calcined at 700 °C are sharp, revealing that the powder is fully transformed to a crystalline state at this temperature. In both cases, the predominant phase present was $Ba_{0.7}Sr_{0.3}TiO_3$. Peaks of $Ba_{0.7}Sr_{0.3}TiO_3$ were identified using PDF card no. 00-44-0093. The PDF card used was

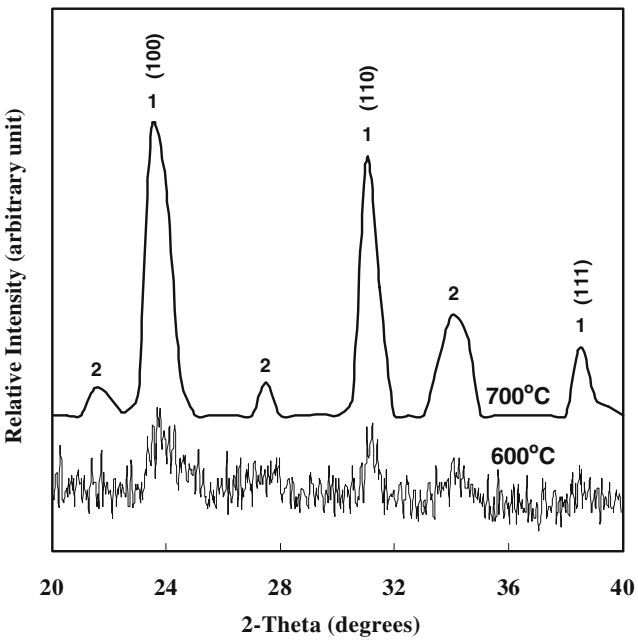

Fig. 2 XRD patterns of BST nanopowder calcined at 600 and 700 °C, separately, for 2 h. $Ba_{0.7}Sr_{0.3}TiO_3$ and $Ba_4Ti_{13}O_{30}$ peaks, observed in these XRD traces, are marked as 1 and 2, respectively

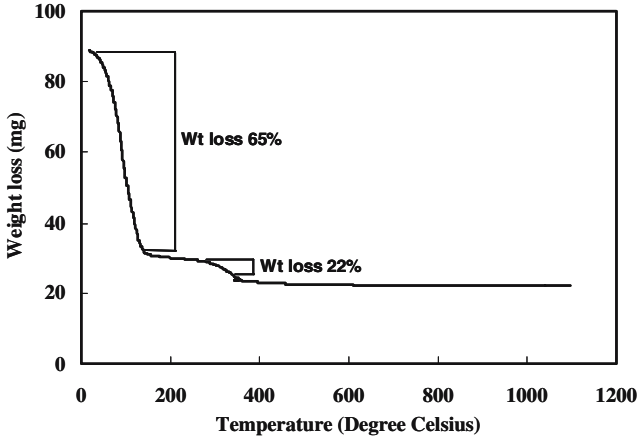

Fig. 3 TGA plot of the as-prepared BST gel. The ramp rate used was 10 °C/min in air ambient with argon as the purge gas

actually for $Ba_{0.77}Sr_{0.23}TiO_3$ as PDF reference for the exact composition synthesized in this work could not be found. The peak corresponding to (100) plane showed the highest intensity and it was seen that the grains did not have any preferred orientation. Small amount of $Ba_4Ti_{13}O_{30}$ phase [PDF # 00-035-0750] was also observed in the XRD pattern. It has been earlier reported that during sol-gel synthesis of barium titanium oxides several intermediate phases form before the transformation of the amorphous phase into perovskite phase [20]. A titania-rich phase was observed during synthesis of $Ba_{0.6}Sr_{0.5}TiO_3$ powder, calcined at 1,150 °C for less than 2 h [13].

It is worth noting that the high surface to volume ratio in nano materials can lead to several interesting properties. The peaks observed in XRD pattern appear slightly shifted towards higher 2-theta angles. This may be due to the decreased interatomic spacing of the small BST nanoparticles. The increased internal pressure in nanoparticles results in an elastic, compressive volume strain and hence, in a linear strain. This may sometimes lead to a reduced lattice parameter or interplanar spacing [21].

Problems arise in multicomponent systems because the precursors hydrolyze at different rates, leading to inhomogeneties. Efforts to synthesize pure BST powders can be broadly divided into following processes. First, synthesis of complex precursors followed by hydrolysis or heat treatment. Khollam et al. [22] synthesized BST powders by synthesizing a barium strontium titanium oxalate (BSTO) precursor followed by pyrolysis at 730 °C for 4 h. They could synthesize $Ba_{0.75}Sr_{0.25}TiO_3$ powder with average powder-particle size of 1 μm. The second process involves the use of cheaper precursors like barium hydroxides or chlorides and is based on hydrothermal synthesis route usually in highly basic solutions. However, the powder recovery in such processes requires successive steps of filtration, washing and drying resulting in modification of Ba/Ti ratio on the particle surface [23]. Tian et al. [24] reported the synthesis of nanoscale magnesium oxide (MgO) wrapped BST powders by a modified hydrothermal process at temperatures as low as 80 °C. In a similar approach, Qi et al. [25] synthesized barium titanate (BT) nanopowders by a process called Direct Synthesis from Solution (DSS).

In order to identify and study the sequence of phase evolution during calcination, XRD analysis was also performed on powder, heat-treated at 400 °C for 2 h. The XRD pattern of this powder predominantly showed the peaks of barium carbonate ($BaCO_3$) and anatase phase of titanium dioxide (TiO_2). Based on these results, the chemical equations leading to $Ba_xSr_{1-x}TiO_3$ phase evolution can be written as:

$$\begin{aligned}
Sr(CH_3COO)_2 &\rightarrow SrCO_3\\
Ba(CH_3COO)_2 &\rightarrow BaCO_3\\
(C_3H_7O)_4Ti &\rightarrow TiO_2.\\
xBaCO_3+(1-x)SrCO_3+TiO_2 &\rightarrow Ba_xSr_{1-x}TiO_3+CO_2.
\end{aligned}$$

3.2 Differential scanning calorimetry and thermal gravimetric analysis

The TGA and DSC plots of the BST gel specimen heated from ambient temperature to 1,100 °C are shown in Figs. 3 and 4, respectively. In Fig. 4, the first endothermic peak on the DSC curve between 50 and 190 °C results from the vaporization of water. This corresponds to a weight loss of about 65% on the TGA curve in Fig. 3. The second exothermic peak on the DSC curve stretching from 320 to 400 °C corresponds to a weight loss of about 22% (Fig. 3) and can be attributed to the dissociation of the acetate and alkoxide organic groups. A third continuous endothermic heat flow region begins from 440 °C and ends at around 550 °C. We believe that in this region the initial formation

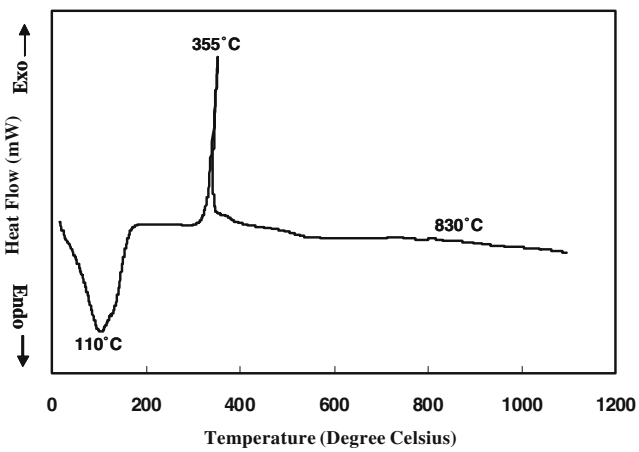

Fig. 4 DSC plot of the as-prepared BST gel from ambient temperature to 1,100 °C. A heating rate of 10 °C/min was used

of $Ba_{0.7}Sr_{0.3}TiO_3$ phase occurs and is followed by its crystallization. This matches well with the XRD patterns (Fig. 2), which shows the presence of partially crystallized $Ba_{0.7}Sr_{0.3}TiO_3$ phase at 600 °C. The DSC curve also shows a broad endothermic region, which starts at 830 °C and stretches till 1,100 °C. This is possibly due to the decomposition of the $Ba_{0.7}Sr_{0.3}TiO_3$ into $Ba_4Ti_{13}O_{30}$ and $Sr_2Ti_5O_{12}$. The decomposition of $Ba_{0.7}Sr_{0.3}TiO_3$ phase has been explained in detail, later in the paper (Section 3.4). The phase evolution as established by DSC/TGA relates very well with the XRD patterns recorded for the powder calcined at 600 and 700 °C (Fig. 2).

3.3 HR-TEM analysis

HR-TEM image of the as-calcined powder at 700 °C is shown in Fig. 5a. Crystallographic planes and ordered arrangement of atoms is visible in this image. The powder was observed to be in form of agglomerates in the dispersed solution. It was also observed that the shape of the powder was not uniform. To determine the average particle size of the powder, measurements were taken along the length and width of several particles and the average of these measurements were calculated. The average particle size of the powder was found to be ~15 nm. The particle size of the powder was also determined using the Scherrer's equation (1) from the recorded XRD pattern, which was found to be ~18 nm, in line with our TEM investigation.

$$\beta = [0.9\lambda/(\langle d\rangle \cos\theta)] \quad (1)$$

where,

λ wavelength of X-rays
θ the Bragg angle,
$\langle d\rangle$ the average particle-size
β the full width at half maximum.

Figure 5b is a magnified TEM image showing clear lattice fringes matching the (100) lattice plane of the $Ba_{0.7}Sr_{0.3}TiO_3$ powder in cubic phase. It is well known that the lattice images are interference patterns between the direct beam and diffracted beams in HR-TEM and that the spacing of a set of fringes is proportional to the lattice spacing, when the corresponding lattice planes meet the Bragg's condition. The calculated interplanar distance from the magnified image was 0.384 nm comparing well against the standard interplanar distance of 0.396 nm for cubic $Ba_{0.6}Sr_{0.4}TiO_3$ (PDF # 00-34-0411) in [100] direction. High Resolution TEM shown in Fig. 6 was done to obtain the Selected Area Electron Diffraction (SAED) pattern of the BST nanopowder. Presence of concentric rings in the diffraction pattern confirms the polycrystallinity of $Ba_{0.7}Sr_{0.3}TiO_3$ powder.

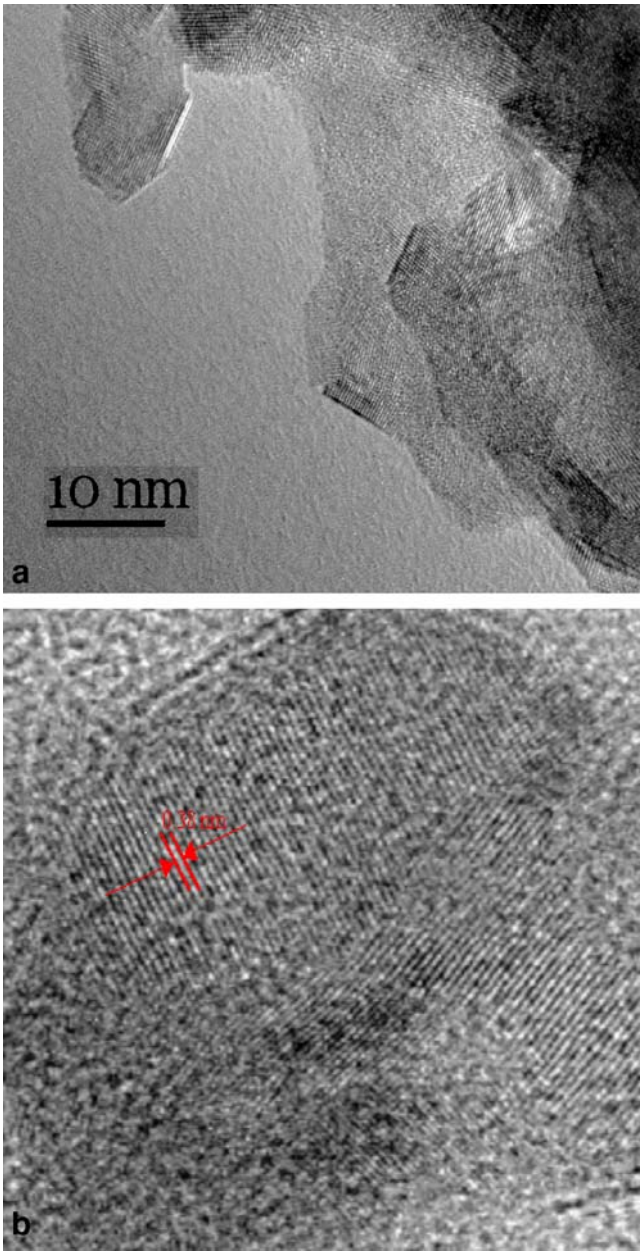

Fig. 5 **a** TEM micrograph of BST powder calcined at 700 °C. **b** TEM micrographs showing lattice fringes and interplanar distance (0.38 nm) of $Ba_{0.7}Sr_{0.3}TiO_3$ phase

3.4 Effect of sintering on phase composition/transformation

Dense nano-BST structures, processed via uniaxial compaction, were sintered at 950, 1,000, 1,050 and 1,100 °C, separately, for 2 h to study the effects of elevated temperature on phase composition/transformation and the densification behavior of the nanopowder. Figure 7 presents the average geometric sintered density (ρ_g) of sintered BST and the corresponding volume shrinkage as a function of sintering temperature. It was observed that the density of

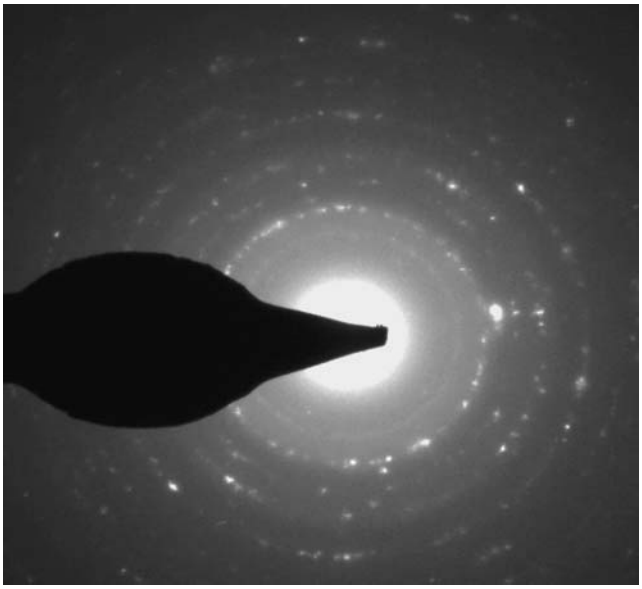

Fig. 6 SAED pattern of the BST powder calcined at 700 °C. Concentric rings confirm presence of crystalline powder

the sintered structures increased from 2.02 g/cm^3 at 950 °C to 2.22 g/cm^3 at 1,000 °C. On further increase of temperature, the sintered density decreased. Overall, it was observed that density of nano-BST could not be improved significantly by pressureless sintering in this temperature range. To our knowledge, densification characteristics of nanocrystalline BST, prepared by sol-gel route, at elevated temperature have not been reported. Here we present an explanation of the densification characteristics of nano-BST based on the XRD analysis of the sintered ceramics. The XRD patterns of nano-BST sintered at 950, 1,000, 1,050 and 1,100 °C are shown in Fig. 8. The XRD results presented in Fig. 8 clearly indicate that even the lowest sintering temperature of 950 °C could change the phase purity of nano-BST. The predominant phase present in nano-BST powder was $Ba_{0.7}Sr_{0.3}TiO_3$, which had possibly decomposed into two separate phases viz., $Ba_4Ti_{13}O_{30}$ [PDF # 00-035-0750] and $Sr_2Ti_5O_{12}$ [PDF # 00-052-1348] at elevated temperature. $Ba_4Ti_{13}O_{30}$, which was present as a minor phase at 700 °C gained in intensity at elevated sintering temperatures. Both of these phases have orthorhombic crystal structure. As can be clearly seen in Fig. 8 that with an increase in temperature from 1,000 to 1,100 °C the peaks of $Ba_4Ti_{13}O_{30}$ and $Sr_2Ti_5O_{12}$ phases increase in intensity with a corresponding decrease in intensity of $Ba_{0.7}Sr_{0.3}TiO_3$ phase peaks. This indicates that the proportions of the dissociated phases increase with increase in temperature and at about 1,100 °C the dissociation is almost complete. The peaks of the dissociated phases are obtained even at 950 °C indicating that the dissociation of the parent phase starts at a temperature lower than 950 °C. B. K. Lee and his coworkers [26] reported the presence of $Ba_4Ti_{13}O_{30}$ in BST powder synthesized by ball milling. They observed an increase in the content of $Ba_4Ti_{13}O_{30}$ phase with the increase in the ratio of Sr:(Sr+Ba) from 0.245 to 0.70 for BST powder sintered at 1,200 °C. In another investigation on doped BST ceramics, $Ba_6Ti_{17}O_{40}$ and $Ba_2TiSi_2O_8$ secondary phases were observed [27].

To qualitatively analyze the percentage of various phases present in the sintered structures, we compared their 100% peak intensity calculated using XRD data. The

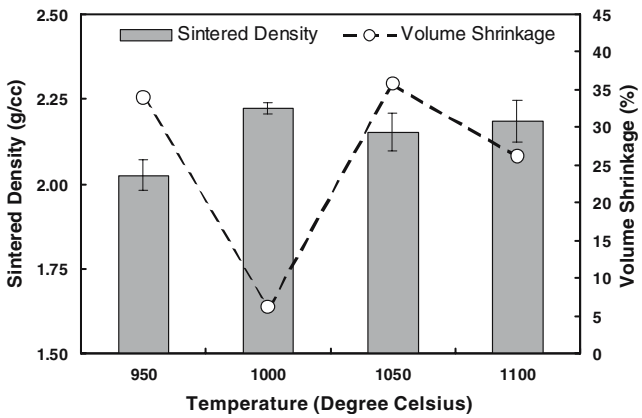

Fig. 7 Effects of sintering on densification of nanocrystalline BST

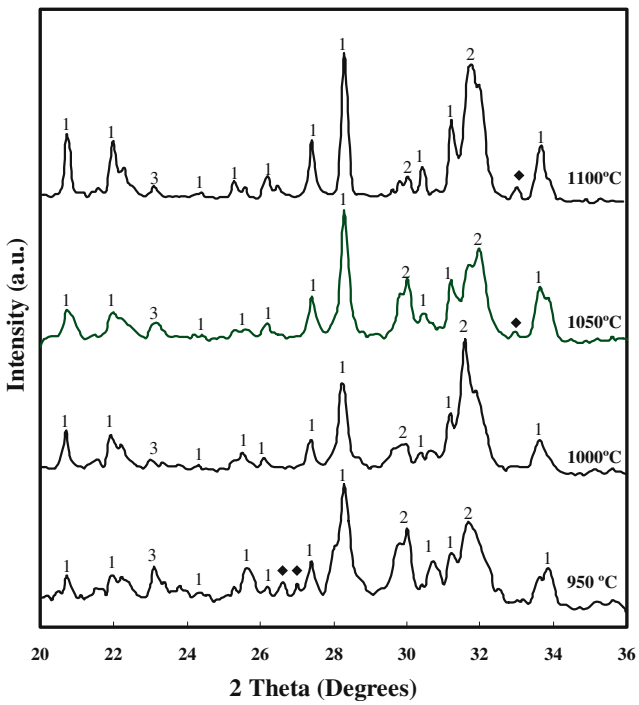

Fig. 8 XRD patterns of sintered BST at 950, 1,000, 1,050 and 1,100 °C, separately, for 2 h. Peaks of $Ba_4Ti_{13}O_{30}$, $Sr_2Ti_5O_{12}$ and $Ba_{0.7}Sr_{0.3}TiO_3$ phases, observed in these XRD traces, are marked as 1, 2 and 3, respectively; whereas *filled diamond* represents unknown peaks

maximum value of peak height corresponding to the various phases present in that composition was recorded and percentage of phases present was calculated using Eq. 2

$$\%\text{phase I} = 100 \times [\text{maximum peak height of phase I}/ (\text{Summation of the maximum peak heights of all the phases present})] \quad (2)$$

We selected 950 and 1,000 °C heat-treated pellets for analysis as we observed the highest sintered density at 1,000 °C. Based on Eq. 2, the percentage of $Ba_{0.7}Sr_{0.3}TiO_3$, $Ba_4Ti_{13}O_{30}$ and $Sr_2Ti_5O_{12}$ phases present in the structures sintered at 950 °C were 5, 55 and 40%, respectively. Whereas, the percentage of these phases present in the structures sintered at 1,000 °C were calculated to be 2, 37 and 61%, respectively. These results can also be used to explain the poor densification behavior of nano-BST observed in this work. We used the calculated results on phase percentage to approximate the theoretical density (ρ_{th}) of sintered structures consisting of these phases viz., $Ba_{0.7}Sr_{0.3}TiO_3$, $Ba_4Ti_{13}O_{30}$ and $Sr_2Ti_5O_{12}$, using the rule of mixture. The theoretical density of $Ba_{0.7}Sr_{0.3}TiO_3$, $Ba_4Ti_{13}O_{30}$ and $Sr_2Ti_5O_{12}$ phases are 5.75, 4.6 and 2.428 g/cm^3, respectively (based on PDF cards). Based on this information, the calculated theoretical density of the structures sintered at 950 and 1,000 °C should be 3.76 and 3.34 g/cm^3, respectively. The sintered density of the pellets measured at 950 and 1,000 °C were 2.02 and 2.22 g/cm^3, respectively. The results indicate that $Ba_4Ti_{13}O_{30}$ and $Sr_2Ti_5O_{12}$ phases are competing for dominance at elevated temperatures and higher percentage of $Sr_2Ti_5O_{12}$ phase in the powder favors better densification. Based on our work, it is seen that that heat treatment of nano $Ba_{0.7}Sr_{0.3}TiO_3$ above 950 °C is not favorable and should be avoided as elevated temperature may cause dissociation during processing of structures and nano films.

It is known that that the solution synthesis of oxides and hydroxides may result in highly unstable materials, which may stabilize by crystallization or result in phase separation upon heating [28]. Multi-element phases are generally stable as long as homogeneity and limited diffusion conditions exist. Loss of homogeneity is affected by residual organics, heating rate and mass of the sample. Dried precipitates in ideal case should not contain any organic materials as their decomposition may lead to exothermic reactions resulting in loss of homogeneity and phase separation. The decomposition of organic components during our synthesis route is complete at around 400 °C as determined by DSC/TGA analysis. The low density seems to be a result of phase decomposition/transformation occurring at elevated temperatures.

It has been reported that the sintering of nanopowder suffers from several challenges such as particle agglomeration, high reactivity, inherent contamination, and loss of nano-features [29]. Use of efficient techniques such as wet compaction, pressure assisted densification processes such as cold isostatic pressing and hot isostatic pressing might improve densification of nano-BST. Qi et al. [30] achieved better sinterability of barium titanate by vapor doping it with B_2O_3. It enhanced sinterability by forming a liquid phase around the grain boundaries. In another work, Liang et al. doped BST ceramics with alumina (Al_2O_3), which reduced its bulk density [31], but it had a strong effect on the dielectric properties and led to a higher tunability.

The full width at half maximum (FWHM) for the most intense peaks of both $Ba_4Ti_{13}O_{30}$ and $Sr_2Ti_5O_{12}$ phases decreased with increase in the temperature from 950 to 1,100 °C. This decrease in FWHM is indicative of an increase in particle size with increasing temperature. It is well known that heat treatment of materials at high temperatures lead to grain growth. This grain growth may sometimes lead to significant increase in grain size and hence alter the properties of the material. Using the Scherrer's formula, the particle size of $Ba_4Ti_{13}O_{30}$ phase was found to be 60.8, 66.74 and 99.95 nm at 950, 1,000 and 1,050 °C, respectively. Similarly, for $Sr_2Ti_5O_{12}$ the particle sizes were calculated to be 21.38 nm, 28.59 nm and 25.32 nm at 950, 1,000 and 1,050 °C, respectively. The smaller size of $Sr_2Ti_5O_{12}$ particles is also evident by their broad peaks in Fig. 8.

3.5 Rietveld analysis of diffraction data

The XRD data of nano-BST heat treated at 700 and 1,000 °C were used for Rietveld refinement using GSAS and graphical user interface Expedt. A pseudo-Voight function was used as the profile function in GSAS. Prior to the Rietveld phase analysis one should have a preliminary idea of the number, name, crystal structure and space group of the phases present. To our knowledge, the required data of all the phases seen in the XRD patterns is not available in literature. Therefore, certain assumptions and simplifications were made to perform the analysis. The space group of $Ba_{0.7}Sr_{0.3}TiO_3$ is unknown; therefore we used $Ba_{0.77}Sr_{0.23}TiO_3$ [PDF#00-044-0093] and $Ba_{0.6}Sr_{0.4}TiO_3$ [PDF#00-034-0411] with space group P4 mm and Pm-3 m, respectively. $Ba_4Ti_{13}O_{30}$ belongs to Cmma space group [32] and was used as such. The space group of $Sr_2Ti_5O_{12}$ phase is unknown and therefore, was not analyzed.

Figures 9 and 10 show the Rietveld plots of nano-BST heat-treated at 700 and 1,000 °C, respectively without any least square refinement. To obtain a better fit of the curve least square refinement was performed on the Rietveld plot of the powder heat treated at 1,000 °C with the background function changed to # 5 with 3 coefficients. The least square refined plot is shown in Fig. 11. Only $Ba_4Ti_{13}O_{30}$

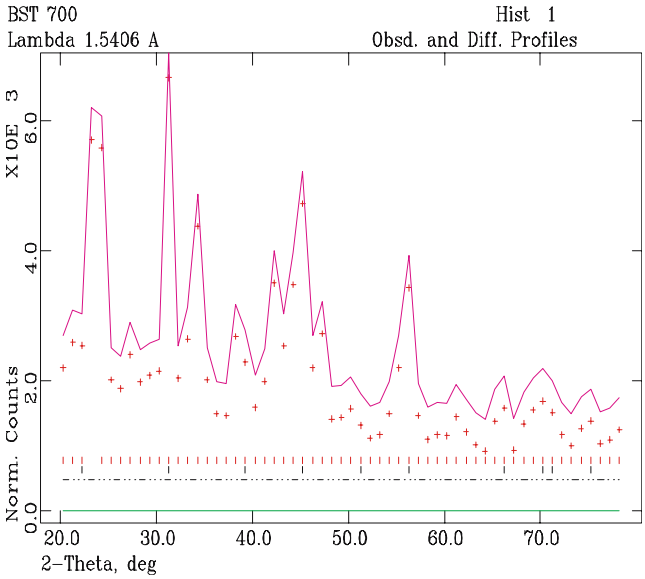

Fig. 9 Rietveld plot for the refinement of BST powder calcined at 700 °C, 2 h. The + and − signs are for observed and calculated intensities, respectively. The toggles just below the curve represent the reflection position of various phases. The uppermost toggle line is for $Ba_{0.7}Sr_{0.3}TiO_3$ followed by $Ba_4Ti_{13}O_{30}$

phase was used for least square analysis as the complete information on other two phases could not be obtained. Peaks of the two unidentified peaks in Figs. 10 and 11 near 22 and 30° are possibly of $Sr_2Ti_5O_{12}$ phase, in accordance with the XRD analysis. The experimental peaks as seen in Rietveld refinement plots are in agreement with the calculated peak positions and intensities, which confirm our XRD phase analysis.

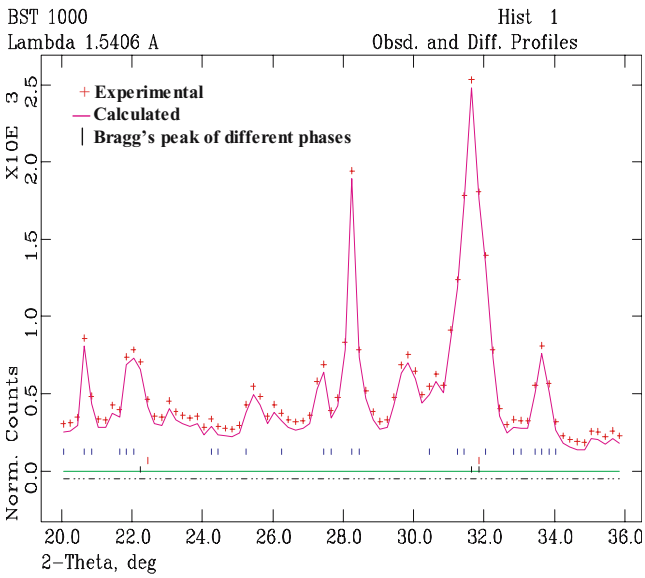

Fig. 10 Rietveld plot for the refinement of BST powder heat treated at 1,000 °C, 2 h. The + and − signs are for observed and calculated intensities respectively. The toggles just below the curve represent the reflection position of various phases. The uppermost toggle line is for $Ba_4Ti_{13}O_{30}$, followed by $Ba_{0.6}Sr_{0.4}TiO_3$ and $Ba_{0.7}Sr_{0.3}TiO_3$

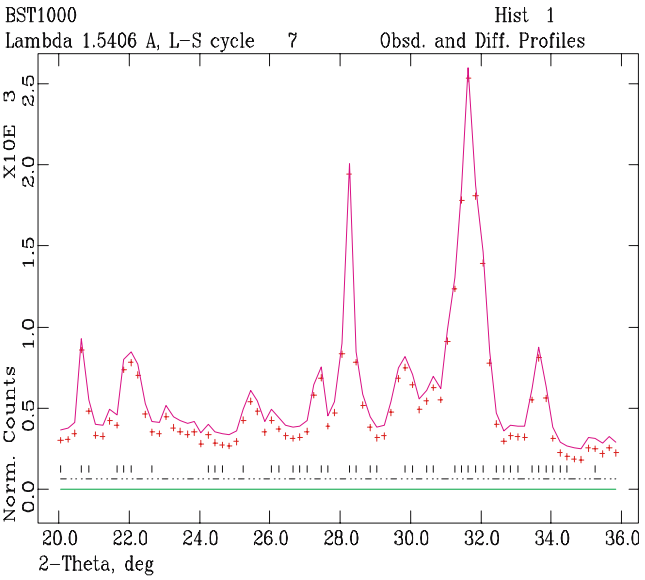

Fig. 11 Rietveld plot for the refinement of BST powder heat treated at 1,000 °C, 2 h with least square refinement. The background function was changed to function # 5 with 3 coefficients. The toggles used here are only for $Ba_4Ti_{13}O_{30}$ phase

4 Conclusions

Nanocrystalline $Ba_{0.7}Sr_{0.3}TiO_3$ powder of average size 15 nm was synthesized via sol gel route. Processing parameters were optimized and the phase evolution during synthesis was studied. It was found that the carbonates of the starting chemicals react to form $Ba_{0.7}Sr_{0.3}TiO_3$ phase at around 600 °C. Complete crystallization was achieved at 700 °C where the phase composition is predominantly $Ba_{0.7}Sr_{0.3}TiO_3$ with a small fraction of $Ba_4Ti_{13}O_{30}$. Phase evolution, as observed in the XRD patterns were consistent with our findings from DSC analysis of the BST gel. Grain size calculated from the XRD pattern was 18 nm, in line with our TEM investigation. The interplanar distance in the BST nano-grains was found to be 0.384 nm based on our TEM analysis. Effects of elevated sintering temperature (950–1,100 °C) on consolidated nano-BST powder were seen to have undesirable outcome—significant phase transformation occurs in this temperature range with the predominant phases being $Ba_4Ti_{13}O_{30}$ and $Sr_2Ti_5O_{12}$ and a small fraction of $Ba_{0.7}Sr_{0.3}TiO_3$. Therefore, we can conclude that it is difficult to maintain the phase purity of nano-$Ba_{0.7}Sr_{0.3}TiO_3$ at elevated temperatures. The sol-gel process developed in this research can be used to deposit nano thin films of BST for their potential application in tunable ferroelectric devices.

Acknowledgement We would like to offer our sincere thanks to Prof. Helge Heinrich of Advanced Materials Processing and Analysis Center (AMPAC) and the Department of Physics for his help with TEM analysis. We also express our earnest gratitude to Mr. Ankush Halbe and Mr. Narayana Garimella of AMPAC and the Department of Mechanical, Materials and Aerospace Engineering for their experimental support.

References

1. X.X. Xi, H.C. Li, W. Si, A.A. Sirenko, I.A. Akimov, J.R. Fox, A. M. Clark, J. Hao, J. Electroceramics **4**(2/3), 393 (2000)
2. M.W. Cole, P.C. Joshi, M.H. Ervin, J. Appl. Phys. **89**(11), 6336 (2001)
3. P.C. Joshi, M.W. Cole, Appl. Phys. Lett, **77**(2), 289 (2000)
4. I.P. Koutsaroff, T. Bernacki, M. Zelner, A. Cervin-Lawry, A. Kassam, P. Woo, L. Woodward, A. Patel, Mater. Res. Soc. Symp. Proc. **784**, 319 (2004)
5. A.K. Tagantsev, V.O. Sherman, K.F. Astafiev, J. Venkatesh, N. Setter, J. Electroceramics **11**, 5 (2003)
6. K.T. Kim, C.-I. Kim, Thin Solid Films **472**, 26–30 (2004)
7. D. Tahan, A. Safari, L.C. Klien, IEEE, CH 3416-50-7803-1847-1/ 95 (1995)
8. M. Jain, S.B. Majumder, R.S. Katiyar, A.S. Bhalla, Thin Solid Films **447**–**448**, 537 (2004)
9. F.W. Van Keuls, C.H. Mueller, R.R. Romanofsky, J.D. Warner, F. A. Miranda, H. Jiang, NASA/TM-2002-210906/ REV1
10. M.W. Cole, P.C. Joshi, M.H. Ervin, M.C. Wood, R.L. Pfeffer, Thin Solid Films **374**, 34 (2000)
11. H. Gleiter, J. Weissmuller, O. Wollersheim, R. Wurschum, Acta Mater. **49**, 737 (2001)
12. J.F. Chen, Z.G. Shen, F.T. Liu, X. L. Liu, J. Yun, Scr. Mater. **49**, 509 (2003)
13. B. Su, J.E. Holmes, B.L. Cheng, T.W. Button, J. Electroceramics **9**, 111 (2002)
14. I. Packia Selvam, V. Kumar, Mater. Lett. **56**, 1089 (2002)
15. C. Shen, Q.F. Liu, Q. Liu, Mater. Lett. **58**, 2302 (2004)
16. T. Hu, H. Jantunen, A. Uusimaki, S. Leppavuori, Mater. Sci. Semicond. Process. **5**, 215 (2003)
17. C. Suryanarayana, C.C. Koch, Hyperfine Interact. **130**, 5 (2000)
18. H.J. Hwang, T. Nagai, M. Sando, M. Toriyama, K. Niihara, J. Eur. Ceram. Soc. **19**, 993 (1999)
19. A.C. Larson, R.B. Von Dreele, *General Structure Analysis System (GSAS)*, Los Alamos National Laboratory Report LAUR 86-748 (2004)
20. S.B. Majumder, M. Jain, A. Martinez, R.S. Katiyar, F.W. Van Keuls, F.A. Miranda, J. Appl. Phys. **90**(2), 896 (2001)
21. R. Kelsall, I. Hamley, M. Geoghegan (eds.), *Nanoscale Science and Technology* (Wiley, Chichester, England, 2005)
22. Y.B. Khollam, S.B. Deshpande, H.S. Potdar, S.V. Bhoraskar, S.R. Sainkar, S.K. Date, Mater. Charact. **54**, 63 (2005)
23. J.F. Bocquet, K. Chhor, C. Pommier, Mater. Chem. Phys. **57**, 273 (1999)
24. H.Y. Tian, J.Q. Qi, Y. Wang, J. Wang, H.L.W. Chan, C.L. Choy, Nanotechnology **16**, 47 (2005)
25. J. Qi, L. Li, Y. Wang, Z. Gui, J. Cryst. Growth **260**, 551 (2004)
26. B.K. Lee, Y. Jung, S.J.L. Kang, J. Nowotny, J. Am. Ceram. Soc. **86**(1), 155 (2003)
27. P. Bomlai, N. Sirikulrat, T. Tunkasiri, Mater. Lett. **59**, 118 (2005)
28. J.R. Groza, Nanostruct. Mater. **12**, 987 (1999)
29. P. Barboux, P. Griesmar, F. Ribot, L. Mazerolles, J. Solid State Chem. **117**, 343 (1995)
30. J.Q. Qi, W.P. Chen, Y. Wang, H.L.W. Chan, L.T. Li, J. Appl. Phys. **96**(11), 6937 (2004)
31. X. Liang, W. Wu, Z. Meng, Mater. Sci. Eng., B **99**, 366 (2003)
32. E. Tillmanns, Inorg. Nucl. Chem. Lett. **7**(12), 1169 (1971)